Progress In Electromagnetics Research M, Vol. 5, 137–152, 2008

THREE-DIMENSIONAL RECONSTRUCTION FROM TIME-DOMAIN ELECTROMAGNETIC WAVES

H. Zhou, D. L. Qiu, J. S. Shen, and G. F. Li †

State Key Laboratory of Petroleum Resources and Prospecting
China University of Petroleum Beijing
Beijing 102249, China

Abstract—An iterative time-domain algorithm for reconstructing three-dimensional (3-D) objects is presented, using normalized microwave data. The incident waveform information is excluded from the cost functional by normalizing the observed and calculated fields in the frequency domain. The exciting pulse used in the reconstruction can be freely selected by considering the bandwidth of the received data. Two numerical examples are shown to demonstrate that the proposed method can rebuild an inhomogeneous object from noisy data where different waveforms in the observation and reconstruction are used. Two normalized data sets from synthetic observed data and calculated data for a known model are illustrated too.

1. INTRODUCTION

Various inversion methods in the frequency domain [1–14] and time domain [15–21] that are suitable for large-size and high-contrast objects have been developed in the last twenty years. For the frequency domain methods there are Born and distorted Born iterative method, Newton-Kantorovitch method, contrast source and modified contrast source inversion method, local shape function method, etc. For the time domain methods there are layer-stripping method, local shape function method, forward-backward time-stepping method, etc. There are several approaches in the frequency domain to reconstruct 3-D objects imbedded in a homogeneous medium or in layered media [11–14], while in the time domain, few 3-D reconstruction examples exist.

† All the authors are also with Key Laboratory of Geophysical Prospecting, China National Petroleum Corporation, Beijing 102249, China

We have proposed a forward-backward time-stepping method for reconstructing electrical properties of dielectric objects using time-domain data and have shown the successful reconstruction of a lossless 3-D object [20] and lossy medium [21]. In the forward-backward time-stepping algorithm, the gradients of the cost functional with respect to the unknown parameters can be expressed explicitly by introducing an adjoint field. In those papers [20–23], the waveform of an incident pulse to the feeding point in the observation was supposedly known before the reconstructions. For the time-domain observations, it is not easy to obtain the exact waveform of the incident pulse required in the reconstructions.

In this paper, based on the forward-backward time-stepping method, we discuss a reconstruction method without requiring the incident waveform information by normalization under an assumption that the received data can be expressed as the convolution of the responses of a transmitting antenna, a receiving antenna, the media in which the microwave propagates, and the incident pulse [24]. A cost functional that is the energy of residuals between the normalized computed and observed fields is defined. The gradients of the cost functional with respect to unknown parameters are derived. The optimization of the cost functional can be achieved by the conjugate gradient method. In this proposed reconstruction method, the deduction of the incident pulse is avoided.

Two reconstruction examples using one component of the electric field are illustrated. Different exciting waveforms are used in the observation and reconstruction. An inhomogeneous and a homogeneous object are reconstructed from noisy data with signal-to-noise ratio (SNR) of 15 dB and 10 dB respectively.

The rest of this paper contains sections on the normalized inverse problem, numerical examples of reconstruction, numerical examples of normalization, and conclusions. In the normalized inverse problem section, the cost functional of the inverse scattering problem is defined, and its gradients with respect to unknown parameters are given. In the numerical examples sections, reconstruction results from noisy data are presented, and normalized data from synthetic observed and computed data are illustrated.

2. NORMALIZED INVERSE PROBLEM

The field data $v_{3m}(\mathbf{p}; \mathbf{r}_n^r, t)$, in general, may be expressed as [24]

$$v_{3m}\left(\mathbf{p}; \mathbf{r}_n^r, t\right) = R_m(t) * P_m\left(\mathbf{p}; \mathbf{r}_n^r, t\right) * J_m(t) * R_n(t), \tag{1}$$

where $*$ represents the convolution for time t; $R_m(t)$ and $R_n(t)$ are the functions of the transmitter and the receiver; $P_m(\mathbf{p};\mathbf{r}_n^r,t)$ is the impulse response of the media at the nth receiver position attributed from a source $J_m(t)$ at the mth source position; $\mathbf{p}=(\varepsilon_r \;\; \mu_r \;\; \eta\sigma)^t$ is the electrical parameters of the media. In the frequency domain (1) is written as

$$v_{3m}\left(\mathbf{p};\mathbf{r}_n^r,\omega\right)=R_m\left(\omega\right)P_m\left(\mathbf{p};\mathbf{r}_n^r,\omega\right)J_m(\omega)R_n(\omega). \tag{2}$$

By normalizing (2) using the received signal, for example, at $\mathbf{r}_l^r$ $(l=1,2,\cdots,\text{or } N)$, we have

$$v_{3mg}\left(\mathbf{p};\mathbf{r}_n^r,\omega\right)=\frac{v_{3m}\left(\mathbf{p};\mathbf{r}_n^r,\omega\right)}{v_{3m}(\mathbf{p};\mathbf{r}_l^r,\omega)}=\frac{P_m\left(\mathbf{p};\mathbf{r}_n^r,\omega\right)R_n(\omega)}{P_m\left(\mathbf{p};\mathbf{r}_l^r,\omega\right)R_l(\omega)}, \tag{3}$$

which does not contain the source information.

An objective functional without the source waveform information is defined as

$$Q(\mathbf{p})=\int_{-\infty}^{+\infty}\sum_{m=1}^{M}\sum_{n=1}^{N}\left|H\left(\omega\right)\left[v_{3mg}\left(\mathbf{p};\mathbf{r}_n^r,\omega\right)-\tilde{v}_{3mg}\left(\mathbf{r}_n^r,\omega\right)\right]\right|^2 d\omega, \tag{4}$$

where $H(\omega)$ is a bandpass filter used to limit the frequency range of the normalized data. Beyond the range the amplitude of the observed and calculated signal is much smaller than its peak value. $v_{3mg}(\mathbf{p};\mathbf{r}_n^r,\omega)$ is the normalized calculated wave field in the media with a guessed parameter $\mathbf{p}$ and $\tilde{v}_{3mg}(\mathbf{r}_n^r,\omega)$ is the normalized observed one at the receiving position corresponding to the mth source. When the full field $\mathbf{v}_m(\mathbf{p};\mathbf{r}_n^r,t)$ is calculated, a source waveform determined from the band of the observed data, not necessarily the same as the pulse shape in the observation, can be used.

Equation (4) is equivalent to a time-domain functional

$$Q(\mathbf{p})=\int_0^{cT}\sum_{m=1}^{M}\sum_{n=1}^{N}\left|v_{3mgf}\left(\mathbf{p};\mathbf{r}_n^r,t\right)-\tilde{v}_{3mgf}\left(\mathbf{r}_n^r,t\right)\right|^2 d(ct), \tag{5}$$

$$v_{3mgf}\left(\mathbf{p};\mathbf{r}_n^r,t\right)=\mathcal{F}^{-1}\left[H(\omega)\frac{v_{3m}\left(\mathbf{p};\mathbf{r}_n^r,\omega\right)}{v_{3m}\left(\mathbf{p};\mathbf{r}_l^r,\omega\right)}\right], \tag{6}$$

$$\tilde{v}_{3mgf}\left(\mathbf{r}_n^r,t\right)=\mathcal{F}^{-1}\left[H(\omega)\frac{\tilde{v}_{3m}\left(\mathbf{r}_n^r,\omega\right)}{\tilde{v}_{3m}\left(\mathbf{r}_l^r,\omega\right)}\right], \tag{7}$$

$\mathcal{F}^{-1}$ is the inverse Fourier transform. T is the duration of the observed data. The distribution of $\mathbf{p}$ is reconstructed from the received data by minimizing the cost functional (5).

By using the same derivation method as [20, 21], the gradients g_ε, g_μ, $g_{\eta\sigma}$ of $Q(\mathbf{p})$ with respect to ε_r, μ_r and $\eta\sigma$ are given by

$$g_\varepsilon = 2\int_0^{cT}\sum_{m=1}^{M}\sum_{i=1}^{3} w_{mg}^{i}(\mathbf{p};\mathbf{r},t)\,\frac{\partial v_{imf}(\mathbf{p};\mathbf{r},t)}{\partial(ct)}d(ct), \tag{8}$$

$$g_\mu = 2\int_0^{cT}\sum_{m=1}^{M}\sum_{i=4}^{6} w_{mg}^{i}(\mathbf{p};\mathbf{r},t)\,\frac{\partial v_{imf}(\mathbf{p};\mathbf{r},t)}{\partial(ct)}d(ct), \tag{9}$$

$$g_{\eta\sigma} = 2\int_0^{cT}\sum_{m=1}^{M}\sum_{i=1}^{3} w_{mg}^{i}(\mathbf{p};\mathbf{r},t)\,v_{imf}(\mathbf{p};\mathbf{r},t)d(ct), \tag{10}$$

where $w_{mg}^{i}(\mathbf{p};\ \mathbf{r},\ t)=\sum_{n=1}^{N} w_{mng}^{i}(\mathbf{p};\ \mathbf{r},\ t)$. $w_{mng}^{i}(\mathbf{p};\ \mathbf{r},\ t)$ is the ith component of $\mathbf{w}_{mng}(\mathbf{p};\ \mathbf{r},\ t)$, which satisfies

$$\begin{aligned}\mathcal{L}^{*}\mathbf{w}_{mng}(\mathbf{p};\mathbf{r},t) &= u_{mgf}^{\mathrm{I}}(\mathbf{p};\mathbf{r}_n^r,t)\,\delta(\mathbf{r}-\mathbf{r}_n^r)\,\mathbf{i}_z \\ &\quad -u_{mgf}^{\mathrm{II}}(\mathbf{p};\mathbf{r}_n^r,t)\,\delta(\mathbf{r}-\mathbf{r}_l^r)\,\mathbf{i}_z, \qquad (11)\\ \mathbf{w}_{mng}(\mathbf{p};\ \mathbf{r},T) &= \mathbf{0}, \qquad (12)\\ u_{mgf}^{\mathrm{I}}(\mathbf{p};\mathbf{r}_n^r,t) &= \mathcal{F}^{-1}\left[H(\omega)\,u_{mg}^{\mathrm{I}}(\mathbf{p};\mathbf{r}_n^r,\omega)\right], \qquad (13)\\ u_{mgf}^{\mathrm{II}}(\mathbf{p};\mathbf{r}_n^r,t) &= \mathcal{F}^{-1}\left[H(\omega)\,u_{mg}^{\mathrm{II}}(\mathbf{p};\mathbf{r}_n^r,\omega)\right], \qquad (14)\\ u_{mg}^{\mathrm{I}}(\mathbf{p};\mathbf{r}_n^r,\omega) &= \frac{u_{mg}(\mathbf{p};\mathbf{r}_n^r,\omega)}{v_{3m}(\mathbf{p};\mathbf{r}_l^r,\omega)^{*}}, \qquad (15)\\ u_{mg}^{\mathrm{II}}(\mathbf{p};\mathbf{r}_l^r,\omega) &= \frac{v_{3m}(\mathbf{p};\mathbf{r}_n^r,\omega)^{*}\,u_{mg}(\mathbf{p};\mathbf{r}_l^r,\omega)}{v_{3m}^{2}(\mathbf{p};\mathbf{r}_l^r,\omega)^{*}}, \qquad (16)\\ u_{mg}(\mathbf{p};\mathbf{r}_n^r,\omega) &= v_{3mg}(\mathbf{p};\mathbf{r}_n^r,\omega)-\tilde{v}_{3mg}(\mathbf{r}_n^r,\omega), \qquad (17)\end{aligned}$$

where $\mathcal{L}^{*}$ is the adjoint operator [20, 21]; the asterisk represents conjugate. $v_{imf}(\mathbf{p};\ \mathbf{r},\ t)$ is the ith component of $\mathbf{v}_{mf}(\mathbf{p};\ \mathbf{r},\ t)$, which is the filtered $\mathbf{v}_m(\mathbf{p};\ \mathbf{r},\ t)$ satisfying the Maxwell's equations. The optimization of the cost functional (5) is achieved by the conjugate gradient method.

In the derivation of the algorithm, it is supposed that the object is set in a very large homogeneous background medium. There are no reflections from the outer boundaries of the background medium. As a result, the perfect matched layer (PML) absorbing boundary condition is used in both forward and backward FDTD simulations.

3. NUMERICAL EXAMPLES OF RECONSTRUCTION

The configuration of transmitters and receivers of synthetic examples is shown in Figure 1. In free space, there is a 3-D object and 3 circles, the middle circle and the 3-D object are concentric. On each circle, 5 transmitting antenna positions are homogeneously distributed as shown in Figure 1(b). Ten receiving dipoles as shown in Figure 1(a) are set uniformly in a range of 216°. All dipoles are in the z-direction.

For each experiment, such as one example as shown in Figure 1(a), only one transmitting ideal dipole illuminates the object and all 30 receiving ideal dipoles record the z-component of the electric field, including the direct coupling and scattered field. The relative horizontal positions of the transmitter and the receivers are fixed. The positions of the receiving antennas are the same for the transmitting antennas located at the same azimuth. For a transmitting antenna at a certain azimuth, the transmitting and receiving antennas are rotated together to let the transmitting antenna locate in that azimuth. The received z-components of the electric field are used to reconstruct the nonconductive and nonmagnetic object.

The incident current pulse to the transmitting antennas for the synthetic observation data is expressed as

$$J(t) = \frac{d^3}{dt^3} \exp\left[-\alpha^2 (t-\tau)^2\right], \tag{18}$$

where $\tau = \beta\Delta t$, $\alpha = 4/\tau$, $\beta = 132$, Δt is the time interval. The wave shape is shown in Figure 2 as the solid line. The highest frequency at which the spectrum amplitude is 5% of the maximum of the incident pulse is about 4.5 GHz. The corresponding wavelength in the background is $\lambda_{\min} = 6.70$ cm. The dominant frequency of the pulse is about half of the maximum frequency.

For both forward (guessed field) and backward (adjoint field) calculations using the FDTD method, the spatial and temporary steps are $\Delta x = \Delta y = \Delta z = \Delta_S = 3.0$ mm and $\Delta t = 5.66$ ps, respectively. The gap of transmitter-receiver circles is $8\Delta_S$.

The 3-D objects are cubes with size of $14\Delta_S \times 14\Delta_S \times 14\Delta_S$ ($0.63\lambda_{\min} \times 0.63\lambda_{\min} \times 0.63\lambda_{\min}$), and the reconstruction region is a cube with side length of $20\Delta_S$ ($0.90\lambda_{\min}$). The radii of the circles are $25\Delta_S$. The FDTD simulation space is $59\Delta_S \times 59\Delta_S \times 59\Delta_S$ and the duration $T = 550\Delta t$.

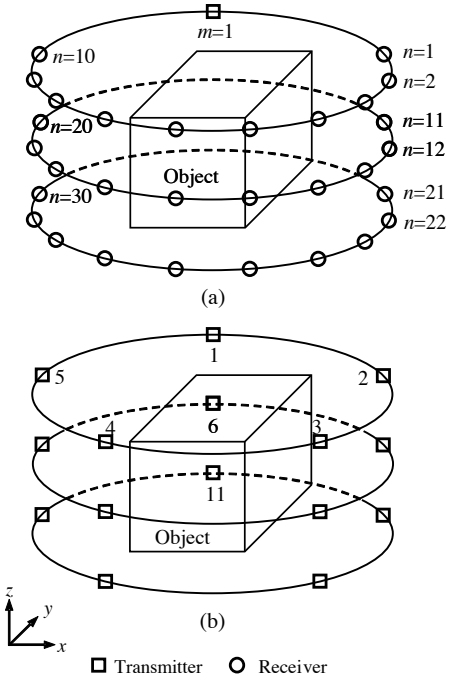

Figure 1. Configuration of transmitting and receiving antennas. (a) A transmitter and its all 30 receivers. (b) Positions of all 15 transmitters.

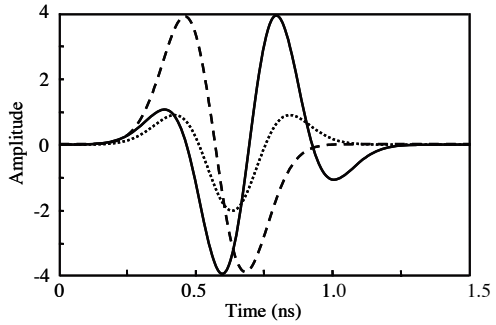

Figure 2. Incident current pulses to the transmitting antennas. The solid line is for observation, and the dotted and dashed lines are for reconstruction.

3.1. Reconstruction of an Inhomogeneous Object

In this example the actual distribution of relative permittivity in the reconstruction region is expressed as

$$\varepsilon_r(i,j,k) = \begin{cases} 1 + 4\cos\dfrac{\pi\,(i-I)}{2l}\cos\dfrac{\pi\,(j-J)}{2l}\cos\dfrac{\pi\,(k-K)}{2l}, \\ i \in [I-l, I+l]\,, j \in [J-l, J+l]\,, k \in [K-l, K+l]\,, \\ 1, \quad \text{elsewhere} \end{cases} \tag{19}$$

where $i, j, k \in [1, 21]$, $l = 7$, $I = J = K = 11$. The maximum value of the relative permittivity is 5. The actual distributions of the relative permittivity of 6 slices perpendicular to the z-axis of the reconstruction cube are shown in Figure 3. Slice 11 passes through the center of the object and the reconstruction cube.

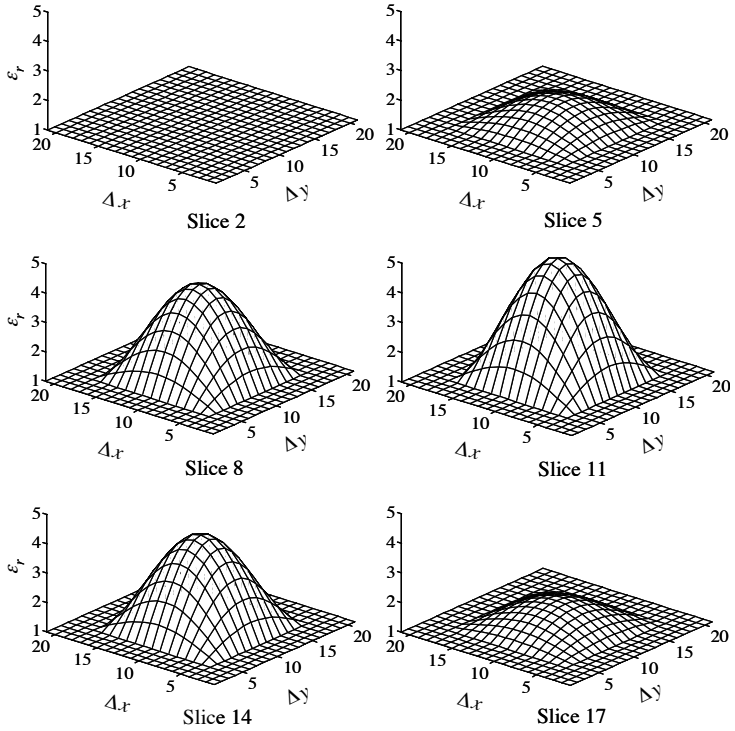

Figure 3. Actual distributions of the relative permittivity of 6 slices perpendicular to the z-axis of the reconstruction cube.

At first, using the same pulse as used in the observation, the reconstruction result from noisy data with SNR = 15 dB is shown in Figure 4. The initial guess of the relative permittivity is set to that of the background. It is known that the object is reconstructed successfully; the influence of the noise is not evident. There is some difference between the actual and reconstructed distributions. In fact, after 20 iterations the object has been roughly reconstructed. Increasing the number of iterations can improve the accuracy of reconstruction. Therefore, the result shown in this paper for this example is at iteration 100. It can be seen from the result that the reconstruction method is stable.

Next, pulses given by (20) and (21), which differs from pulse (18) in the observation, are used in the reconstruction

$$J(t) = \frac{d^2}{dt^2} \exp\left[-\alpha^2 (t-\tau)^2\right], \tag{20}$$

$$J(t) = \frac{d}{dt} \exp\left[-\alpha^2 (t-\tau)^2\right], \tag{21}$$

where $\beta = 121$ and $\beta = 110$ for (20) and (21) respectively. The bandwidth of (20), (21) is the same as that of (18). The wave shapes are shown in Figure 2 as the dotted and dashed lines.

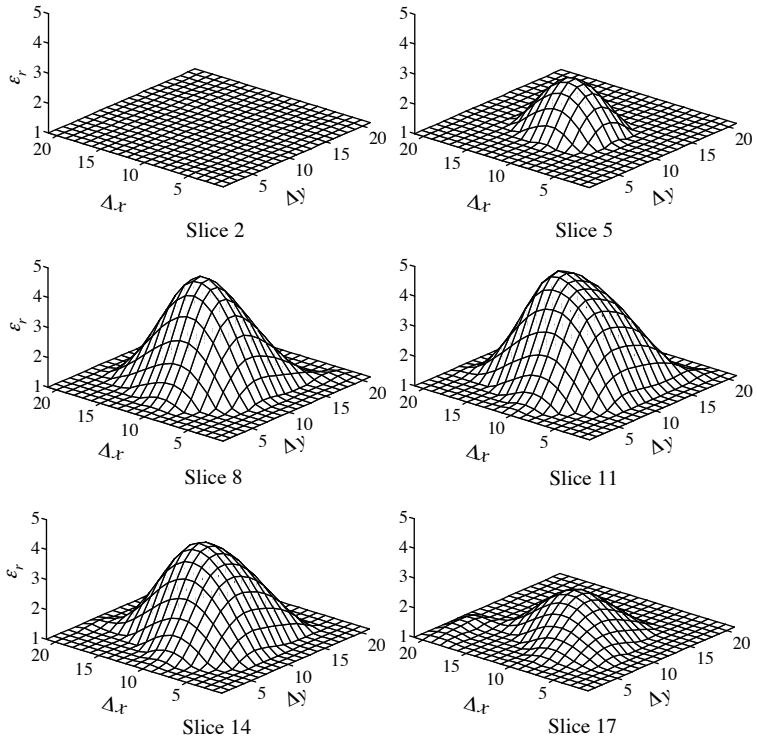

Figure 4. Reconstructed distributions of the relative permittivity of the slices at the 100th iteration from noisy data with SNR = 15 dB. The pulse used in reconstruction is the solid one in Figure 2, which is the same as that in observation.

Figure 5 illustrates the reconstructed result at the 100th iteration from the noisy data using pulse (20) and Figure 6 is the result using pulse (21). Comparing Figures 5 and 6 with Figure 4 it is known

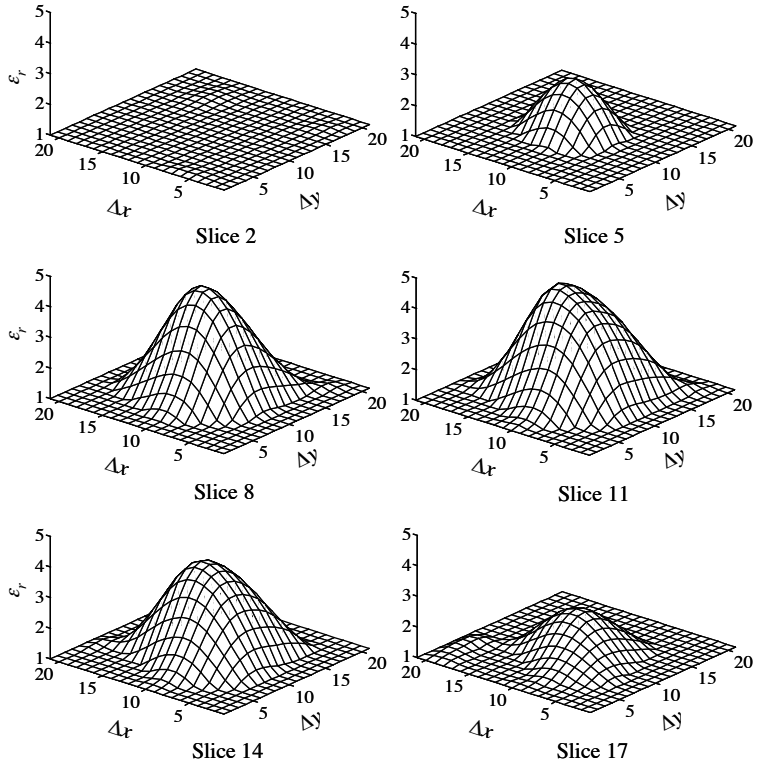

Figure 5. Reconstructed distributions of the relative permittivity of the slices at the 100th iteration from noisy data with SNR = 15 dB. The pulse used in reconstruction is the dotted one in Figure 2.

that the reconstructed object is almost the same by using the exact and different pulses. It means that the reconstructed result is not influenced by the wave shape of the incident pulse.

Each iteration takes about 8 min on a personal computer with Intel Core 2 Duo CPU 2.4 GHz, 4 GB RAM, and Windows Vista operating system.

3.2. Reconstruction of a Homogeneous Object

The setup and the size of the object are the same as those of the inhomogeneous example. The distribution of relative permittivity is

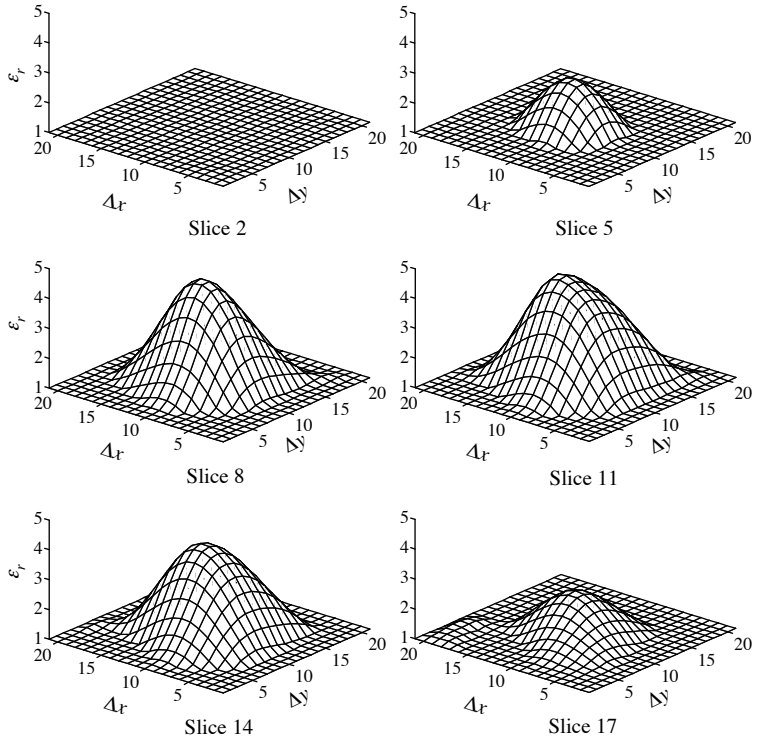

Figure 6. Reconstructed distributions of the relative permittivity of the slices at the 100th iteration from noisy data with SNR = 15 dB. The pulse used in reconstruction is the dashed one in Figure 2.

given by

$$\varepsilon_r(i,j,k) = \begin{cases} 5, i \in [I-l, I+l], j \in [J-l, J+l], k \in [K-l, K+l] \\ 1, \quad \text{elsewhere} \end{cases}. \tag{22}$$

The reconstructed result is shown in Figure 7 from noisy data of SNR = 10 dB after 55 iterations. The incident waveform in the reconstruction is given by (20). It is seen from Figure 7 that the homogeneous object is correctly reconstructed. Figure 7 illustrates that the object can be reconstructed from noisy data. However, it is clear that the homogeneous object is not reconstructed as accurately as the smooth model. Although the shapes of the distributions are deformed, it is clear that there is an object in the reconstruction region, and the properties of the object is recognizable. The influence of the noise is clearly seen.

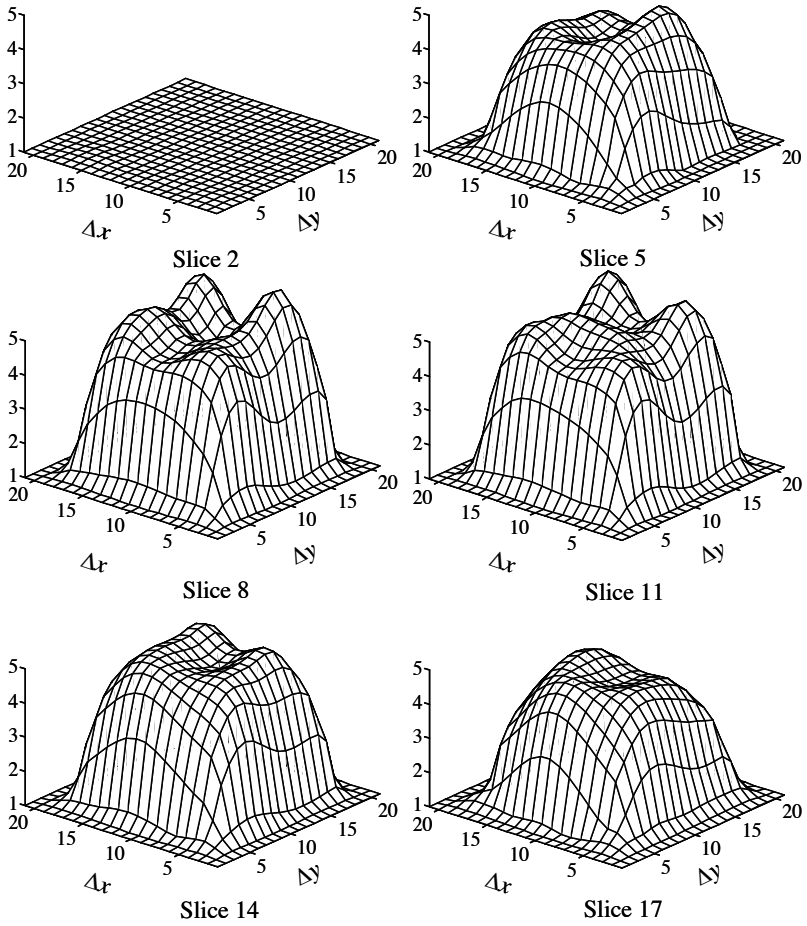

Figure 7. Reconstructed distributions of the relative permittivity of the slices at the 55th iteration from noisy data with SNR = 10 dB.

Figure 8 shows the bandpass filter in (4) in the reconstruction examples. It is determined according to the band of the observed data.

4. NUMERICAL EXAMPLES OF NORMALIZATION

To illustrate the effect of the normalization method, the observed, calculated, and normalized data for the known model in the first example are shown here. In Figures 9(a) and (c), the dotted lines are the calculated data $v_{3m}(\mathbf{p};\ \mathbf{r}_n^r,\ t)$; the dashed lines are the noise-

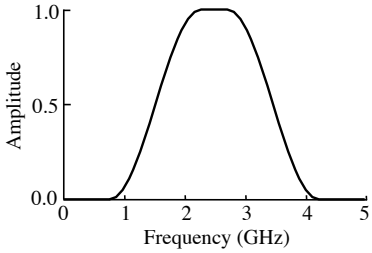

Figure 8. The bandpass filter used in the reconstruction examples.

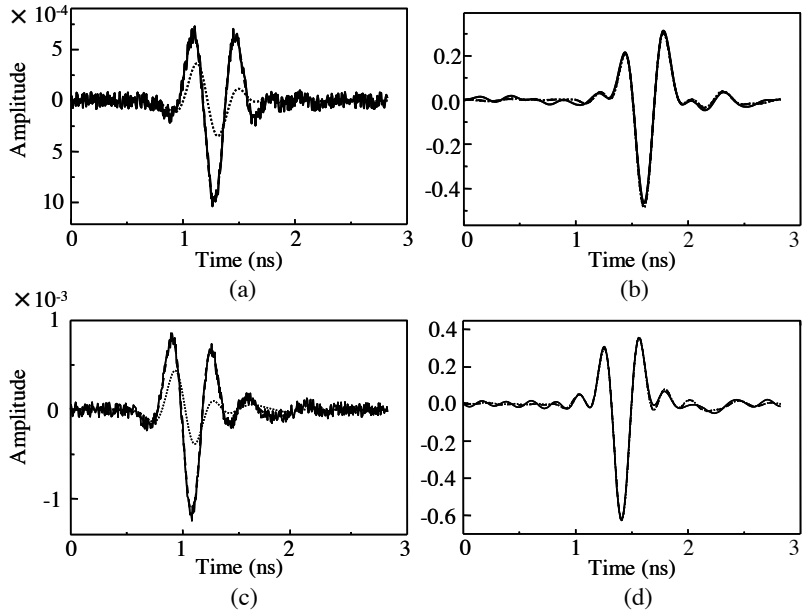

Figure 9. Examples of data normalization. In (a) and (c) are calculated (dotted line) and observed noise-free (dashed line) and noisy data (solid line), in (b) and (d) are filtered normalized data from the calculated data (dotted line), noise-free observed data (dashed line), and noisy observed data (solid line). (a) and (b) are of $m = 1$, $n = 7$, and (c) and (d) are of $m = 1$, $n = 30$.

free "observed" data $\tilde{v}_{3m}(\mathbf{r}_n^r,\ t)$, and the solid lines show the noisy observed data with SNR = 15 dB. In Figures 9(b) and (d), the dotted lines are the filtered normalized data $v_{3mgf}(\mathbf{p};\ \mathbf{r}_n^r,\ t)$ given by (6) with $l = 1$ (see Figure 1); the dashed lines are the filtered normalized noise-free data $\tilde{v}_{3mgf}(\mathbf{r}_n^r,\ t)$ calculated by (7); and the solid lines show

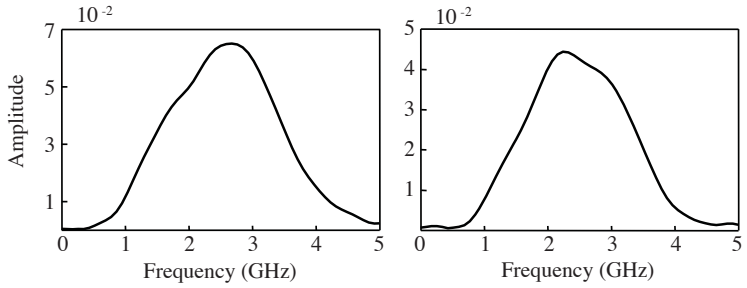

Figure 10. Exmaples of amplitude spectra of "observed" noisy data. (a) is of $m = 1,\ n = 1$, and (b) is of $m = 1,\ n = 7$.

the filtered normalized noisy observed data. In the computation of the calculated data, pulse (20) is used, while in the calculation of the observed data, pulse (18) is used. Figures 9(a) and (b) are for $m = 1$ and $n = 7$ and Figures 9(c) sand (d) are for $m = 1$ and $n = 30$. From the normalized noise-free and noisy data it can be seen that the normalization is effective.

Figure 10 shows the amplitude spectra of two received "observed" noisy signals of the first reconstruction example. Figure 10(a) is of $m = 1,\ n = 1$, and (b) is of $m = 1,\ n = 7$, whose time domain signal is the solid line in Figure 9(a). There is no zero amplitude in the band of a bandpass filter whose band is 0.69–4.14 GHz, out of this band the filtered amplitude is zero.

5. CONCLUSIONS

We propose a method that the incident waveform information can be removed by normalizing the observed data by the received signal at a certain position. This technique differs from the calibration method in the frequency domain data acquisition that is for calibrating the system [25], or to approximate, for example, horn antennas by line sources [26]. However, this method is for excluding the information of the incident pulse. The reconstruction of a three-dimensional homogeneous and inhomogeneous lossless and nonmagnetic objects has succeeded, using normalized noisy data. In the reconstruction, the exact incident waveform information is not required. As a result, the difficult process of deducting the incident pulse can be avoided.

There are some interesting and important topics to investigate. For example, how the radiation pattern of antennas and the

gap between the scattering object and the antennas affect the reconstruction results, and what is the relation between the reconstruction accuracy and object size for this algorithm. These are our future research topics.

ACKNOWLEDGMENT

This work was supported in part by the National Natural Science Foundation of China under Grant-in-Aid 40574053, the Program for New Century Excellent Talents in University, China, and the State Key Laboratory of Petroleum Resources and Prospecting, China.

REFERENCES

1. Chew, W. C. and Y. M. Wang, "Reconstruction of two-dimensional permittivity distribution using the distorted Born iterative method," *IEEE Trans. Med. Imag.*, Vol. 9, No. 2, 218–225, 1990.
2. Zaeytijd, D., J. Franchois, A. C. Eyraud, and J. M. Geffrin,"Full-wave three-dimensional microwave imaging with a regularized Gauss-Newton method – Theory and experiment," *IEEE Trans. on Antennas Propagat.*, Vol. 55, No. 11, 3279–3292, 2007.
3. Otto, G. P. and W. C. Chew, "Microwave inverse scattering-local shape function imaging for improved resolution of strong scatterers," *IEEE Trans. Microwave Theory Tech.*, Vol. 42, No. 1, 137–141, 1994.
4. Franchois, A. and C. Pichot, "Microwave imaging-complex permittivity reconstruction with a Levenberg-Marquardt method," *IEEE Trans. Antennas Propagat.*, Vol. 45, No. 2, 203–214, 1997.
5. van Dongen, K. W. A. and W. M. D. Wright, "A full vectorial contrast source inversion scheme for three-dimensional acoustic imaging of both compressibility and density profiles," *The Journal of the Acoustical Society of America*, Vol. 121, 1538–1549, 2007.
6. Bucci, O. M., L. Crocco, T. Isernia, and V. Pascazio, "Inverse scattering problems with multifrequency data: Reconstruction capabilities and solution strategies," *IEEE Trans. Geosci. Remote Sensing*, Vol. 38, No. 4, 1749–1756, 2000.
7. Cui, T. J., Y. Qin,Y. Ye, J. Wu, G. L. Wang, and W. C. Chew, "Efficient low-frequency inversion of 3-D buried objects with large contrasts," *IEEE Trans. Geosci. Remote Sensing*, Vol. 44, No. 1, 3–9, 2006.

8. Pastorino, M., A. Massa, and S. Caorsi, "A microwave inverse scattering technique for image reconstruction based on a genetic algorithm," *IEEE Trans. Instrumentation and Measurement*, Vol. 49, No. 3, 573–578, 2000.
9. Isernia, T., V. Pascazio, and R. Pierri, "On the local minima in a tomographic imaging technique," *IEEE Trans. Geosci. Remote Sensing*, Vol. 39, No. 7, 1596–1607, 2001.
10. Caorsi, S., M. Donelli, D. Franceschini, and A. Massa, "An iterative multiresolution approach for microwave imaging applications," *Microwave Opt. Technol. Lett.*, Vol. 32, No. 5, 352–356, 2002.
11. Joachimowicz, N., C. Pichot, and J. Hugonin, "Inverse scattering: an iterative numerical method for electromagnetic imaging," *IEEE Trans. Antennas Propagat.*, Vol. 39, No. 12, 1742–1752, 1991.
12. Lin, J.-H. and W. C. Chew, "Solution of the three-dimensional electromagnetic inverse problem by the local shape function and the conjugate gradient fast Fourier transform methods," *J. Opt. Soc. Am. A*, Vol. 14, No. 11, 3037–3045, 1997.
13. Abubakar, A., P. M. van den Berg, and B. Kooij, "A conjugate gradient contrast source technique for 3D profile inversion," *IEICE Trans. Electron. E83-C*, 1864–1874, 2000.
14. Song, L. P. and Q. H. Liu, "Fast three-dimensional electromagnetic nonlinear inversion in layered media with a novel scattering approximation," *Inverse Problems*, Vol. 20, 171–194, 2004.
15. Moghaddam, M. and W. C. Chew, "Study of some practical issues in inversion with the Born iterative method using time-domain data," *IEEE Trans. Antennas Propagt.*, Vol. 41, No. 2, 177–184, 1993.
16. Fhager, A., P.Hashemzadeh, and M. Persson, "Reconstruction quality and spectral content of an electromagnetic time-domain inversion algorithm," *IEEE Trans. on Biomedical Eng.*, Vol. 53,1594–1604, 2006.
17. He, S., P. Fuks, and G. W. Larson, "Optimization approach to time-domain electromagnetic inverse problem for a stratified dispersive and dissipative slab," *IEEE Trans. Antennas Propagat.*, Vol. 44, No. 9, 1277–1282, 1996.
18. Yu, W. H. and R. Mittra, "A nonlinear optimization technique for reconstructing dielectric scatterers with possible high contrasts," *Microwave Opt. Technol. Lett.*, Vol. 14, No. 2, 268–271, 1997.
19. Gustafsson, M. and S. He, "An optimization approach to two-dimensional time domain electromagnetic inverse problems,"

Radio Sci., Vol. 35, 525–536, 2000.

20. Takenaka, T., H. Zhou, and T. Tanaka, "Inverse scattering for a three-dimensional object in the time domain," *J. Opt. Soc. Am. A*, Vol. 20, No. 10, 1867–1874, 2003.
21. Zhou, H., M. Sato, T. Takenaka, and G. Li, "Reconstruction from antenna transformed radar data using a time-domain reconstruction method," *IEEE Trans. Geosci. Remote Sensing*, Vol. 45, No. 3, 689–696, 2007.
22. Tanaka, T., N. Kuroki, and T. Takenaka, "Filtered forward-backward time-stepping method applied to reconstruction of dielectric cylinders," *J. Electromagn. Waves Appl.*, Vol. 17, No. 2, 253–270, 2003.
23. Zhou, H., D. L. Qiu, and T. Takenaka, "Reconstructing properties of subsurface from Ground-penetrating radar data," *Progress In Electromagnetics Research Symposium 2007*, 1009–1014, Beijing, China, March 26–30, 2007.
24. Daniels, D. J., *Surface-penetrating Radar*, UK Instit Elect Eng., London, 1996.
25. Broquetas, A., J. Romeu, J. M. Rius, A. R. Elias-Fuste, et al., "Cylindrical geometry: A further step in active microwave tomography," *IEEE Trans. Microwave Theory Tech.*, Vol. 39, No. 5, 836–844, 1991.
26. Bloemenkamp, R. F., A. Abubakar, and P. M. van den Berg, "Inversion of experimental multi-frequency data using the contrast source inversion method," *Inverse Problems*, Vol. 17, 1611–1622, 2001.